Development and validation of the Terrain Stability model for assessing landslide instability during heavy rain infiltration.

1. Alfonso Gutiérrez-Martín[|1|] Miguel Ángel Herrada[|2|], José Ignacio Yenes Gallego[|3|], Ricardo Castedo Ruiz[|4|]

[|1|] Dr. Arquitecto, Escuela Superior de Arquitectura; Universidad de Málaga, España. E-mail: alfgutmar@uma.es

[|2|] Catedrático de Universidad, Escuela Superior de Ingenieros de la Universidad de Sevilla. España. E-mail: herrada@us.es

[|3|] Dr. Ingeniero José Ignacio Yenes Gallego, Jefe de Unidad, Dirección General de Infraestructuras, MINISDEF, Madrid, España. E-mail: jyengal@et.mde.es

[|4|] Dr. Ingeniero Ricardo Castedo Ruiz, Departamento de Ingeniería Geológica y Minera, Universidad Politécnica de Madrid, España. E-mail: ricardo.castedo@upm.es

Abstract

Slope stability is a key topic, not only for engineers but also for politicians, due to the considerable monetary and human losses that landslides can cause every year. In fact, it is estimated that landslides have caused thousands of deaths and economic losses amounting to tens of billions of e6uros per year around the world. The geological stability of slopes is affected by several factors, such as climate, earthquakes, lithology and rock structures, among others. Climate is one of the main factors, especially when large amounts of rainwater are absorbed in short periods of time. Taking into account this issue, we developed an innovative analytical model using the limit equilibrium method supported by a geographic information system (GIS). This model is especially useful for predicting the risk of landslides in scenarios of heavy unpredictable rainfall. The model, hereafter named 'Terrain Stability' or TS is a 2D model, programmed in MATLAB and includes a steady state hydrological term. Many variables measured in the field – topography, precipitation, type of soil – can be added, changed or updated using simple input parameters. To validate the model, we applied it to a real example, that of a landslide which resulted in human and material losses (collapse of a building) at Hundidero, La Viñuela (Málaga), Spain, in February 2010.

Keywords: Rainfall, Slope, Limit equilibrium model, algorithm and critical surface.

1. Introduction

Landslides, one of the natural disasters, have resulted into significant injury and loss to human life and damaged property and infrastructure throughout the world (Varnes, 1996; Parise and Jibson, 2000; Dai et al., 2002; Guha-Sapir et al., 2004; Crozier and Glade, 2005; Kahn, 2005; Toya and Skidmore, 2007; Raghuvanshi et al., 2014; Girma et al., 2015). Normally, heavy rainfall, high relative relief and complex fragile geology with increased manmade activities, have resulted in increased landslide (Gutiérrez-Martín, 2015). It is essential to identify, evaluate and delineate landslide hazard prone areas for proper strategic planning and mitigation (Bisson et al., 2014). Therefore, to delineate landslide susceptible slopes over large

areas, landslide hazard zonation (LHZ) techniques can be employed (Anbalagan, 1992; Guzzetti et al., 1999; Casagli et al., 2004; Fall et al., 2006).

Landslides are resulted because of intrinsic and external triggering factors. The intrinsic factors are mainly; geological factors, geometry of the slope (Hoek and Bray, 1981; Ayalew et al., 2004; Wang and Niu, 2009).

The external factors which generally trigger landslides are rainfall (Anderson, 1985; Collison et al., 2000; Dai and Lee, 2001). Several LHZ techniques have been developed over the past and these can be broadly classified into three categories; expert evaluation, statistical methods and deterministic approaches (Wu and Sidle, 1995; Leroi, 1997; Guzzetti et al., 1999; Inverson, 2000; Crosta and Frattini, 2003; Casagli et al., 2004; Fall et al., 2006; Lu and Godt, 2008; Rossi et al., 2013; Raia et al., 2014; Canili et al., 2018; Zhang et al.; 2018). Within these categories, we want to highlight the empirical models that are based on rainfall thresholds (Wilson, 1997; Aleotti, 2004; Gruzzetti et al., 2007; Martelloni et al., 2011). Each of these LHZ techniques has its own advantage and disadvantage owing to certain uncertainties on account of factors considered or methods by which factor data are derived (Carrara et al., 1995). Limit equilibrium types of analyses for assessing the stability of earth slopes have been in use in geotechnical engineering for many decades. The idea of discretizing a potential sliding mass into vertical slices was introduced in the 20th century. During the following few decades, Fellenius (1936) introduced the Ordinary method of slices (Fellenius, 1936). In the mid1950s Janbu and Bishop developed advances in the method (Janbu, 1954; Bishop, 1955). The advent of electronic computers in the 1960's made it possible to more readily handle the iterative procedures inherent in the method, which led to mathematically more rigorous formulations such as those developed by Morgenstern and Price and by Spencer (Morgenstern and Price, 1965; Spencer, 1967).

Until the 1980s, most stability analyses were performed by graphical methods or by using manual calculators. Nowadays, the quickest and most detailed analyses can be performed using any ordinary computer (Wilkinson et al., 2002). There are other types of software based on the modeling of the probability of occurrence of shallow landslides LHZ, in more extensive areas using GIS technology and 'DEM' (Digital Elevation Model), as is the case of deterministic models like: software TRIGRS, SINMAP, R-SHALSTAB, GEOtop/GEO-FS, R-Slope-stability among others (Montgomery and Dietrich, 1998; Pack et al., 2001; Rigon et al., 2006; Simoni et al., 2008 ; Baum et al., 2008; Mergili et al., 2014a; Mergili et al., 2014b; Michel et al., 2014; Reid et al., 2015; Alvioli and Baum, 2016; Tran et al., 2018). These are widely used models for calculating the time and location of the occurrence of shallow landslides caused by rainfall at the territorial level; some even in three dimensions, in order to obtain a probabilistic interpretation of the factor of safety. Currently other approaches / theoretical studies for landslide prediction are used (for triggering and / or propagation) (Martelloni and Bagnoli, 2014; Martelloni et al., 2017). One of the achievements of the presented study is to discretize the potential slip mass in the critical profile of the slope, once unstable areas have been detected through the 'LHZ' (landslide hazard zonation) programs. The TS calculation tool is not limited to shallow landslides and debris flows, but allows analysis of deep and rotational landslides, which often other models do not accommodate for. We use in our algorithm the

hydrological variable 'r_u' of Spencer, to consider the infiltration of rainfall in the calculation of stability of the considered slope.

Limit equilibrium types of analyses for assessing the stability of earth slopes have been in use in geotechnical engineering for last years. Currently, the vast majority of stability analyses using **this method of equilibrium limit** are performed with commercial software packages like SLIDE V5, SLOPE/W, Phase2, GEO-Slope, GALENA, GSTABL7, GEO5 and GeoStudio, among others (Gonzalez de Vallejo et al., 2002; Acharya et al., 2016a; Acharya et al., 2016b; Johari and Mousavi, 2018). Currently there are other slope stability models based on the theory of limit equilibrium that are still in analysis and testing, as is the case with the SSAP software package (Borselli, 2012), but in this case a general equilibrium method model is applied. Secondly, sometimes for commercial models, the introductions of parameters to perform calculations are not very interactive. For the stability analysis, different approaches can be used, such as the limit equilibrium methods (Cheng et al., 2007; Liu et al., 2015), the finite elements method (Griffiths et al., 2007; Tschuchnigg et al., 2015; Griffiths, 2015) and the dynamic method (Jia et al., 2008), among others. Limit equilibrium methods are well known, and their use is simple and quick. These methods allow us to analyse almost all types of landslides, such us translational, rotational, topple, creep and fall, among others (Zhou and Cheng, 2013). For the stability analysis, different approaches can be used, such as the limit equilibrium methods (Zhu et al., 2005; Cheng et al., 2007; Verruijt, 2010; Liu et al., 2015), the finite elements method (Griffiths et al., 2007; Tschuchnigg et al., 2015; Griffiths, 2015) and the dynamic method (Jia et al., 2008) among others (SSAP 2012, Slide V5-2018). Also, limit equilibrium methods can be combined with probabilistic techniques [Stead et al., 2000] or with other models, like stability analysis of coastal erosion (Castedo et al., 2012). However, they are limited in general to 2D planes and easy geometries. Numerical methods – finite elements methods – give us the most detailed approach to analysing the stability conditions for the majority of evaluation cases, including complex geometries and 3D cases. Nevertheless, they present some problems, such as their complexity, data introduction, mesh size effect and the time and resources they require (Ramos Vásquez, 2017).

The above-mentioned software packages provide useful tools for determining the stability through the F_S (safety of factor) and for giving the most probable breakage (shearing) surfaces. This technique is fast and allows the field or emergency engineer to make timely decisions. Although this methodology is only available in some current software (Slide V 5.0, STB 2010, Geo-Slope), and based on limit equilibrium methods, it is highly recommended because of its reliability for representing real conditions in the field (Chugh, 1981). This rain infiltration produces a substantial reduction of cohesion (a key soil parameter for stability) that cannot be reproduced by actual software and then several real situations cannot be predicted.

Delft University has developed a well-known and free software programme to analyse landslides, the STB 2010 (Verruijt, 2010). This programme is based on a limit equilibrium technique, using a modified version of Bishop's method to calculate the F_S only for circular failures. It is a user-friendly tool, but it does not allow the calculation of water infiltration on a hillside. This is a critical point, as it is well known that rainfall infiltration is one of the main causes of landslides worldwide (Michel et al., 2015). Reviewing these issues, a new solution must be developed for cases where landslides are linked to heavy rainfall. In this study, we

developed a new model and programmed it using MATLAB. The primary result of this model was a stability index, namely the minimum *Fs,* based on the limit equilibrium technique, in this case the Bishop's method. The model also provides a possible failure curve and surface area, including the infiltration effects, which can be used to coincide with analysis of the actual event as tested with field data. Topographical data can also be introduced into the model from the digital elevation model (DEM) in a GIS.

2. Terrain Stability model development

In the model we developed the Terrain Stability (TS) model, we used the limit equilibrium technique for its versatility, calculation speed and accuracy. An analysis can be done studying the whole length of the breakage (shearing) zone or just small slices. Starting with the original method of slides developed by Petterson and Fellenius (1936), some methods are more accurate and complex (Spencer 1967; Morgenstern and Price, 1965) than others (Bishop, 1955 and Janbú, 1954). Using Spencer's method (Spencer, 1967; Chung, 1986) here would mean dividing our slope into small slices that must be computed together. This method is divided into two equations, one related to the balance of forces and the other to momentum. Spencer's method imposes equilibrium not only for the forces but also for the momentum on the surface of the rupture. If the forces for the entire soil mass are in equilibrium, the sum of the forces between each slice must be also equal to zero. Therefore, the sum of the horizontal forces between slices must be zero as well as the sum of the vertical ones (equations 1 and 2).

$$\sum[Q\cos\theta] = 0 \quad (1)$$

$$\sum[Q\sin\theta] = 0 \quad (2)$$

In this equation, *Q* is the resultant of the pair of forces between slices, and θ is the angle of the resultant (Figure 1). From this, it can be stated that the sum of the moments of the forces between slices around the critical rotation centre is zero, conformed to equation 3:

$$\sum[QR\cos(\alpha-\theta) = 0] \quad (3)$$

When the R is the radius of the curvature, α is the angle of the slope referred to each slice. This takes into account that the sliding surface is considered circular, so the radius of the curvature is constant.

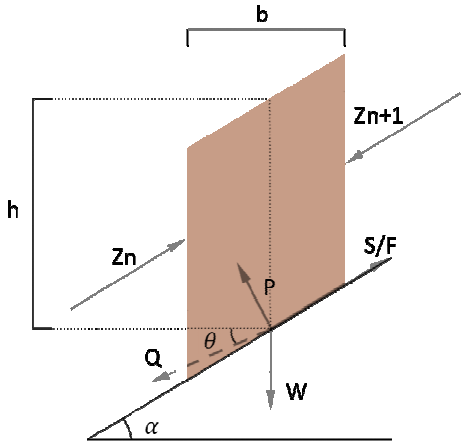

Figure 1. *Representation of the forces acting on a slice, considered in Spencer's method (Spencer, 1967). W is the external vertical loads; Zn and Zn+1 are the forces acting on the left- and right-hand side of each slice, respectively, with their horizontal and vertical components; P and S are the normal and tangential forces at the base of the slice; α is the angle of the slope referred to each slice, b is the slice width and h is the mean height of slice (if the height is not constant).*

These equations must be solved to get the F_S, and tilt angles of the forces among the slices (θ). To solve these equations, an iterative method is required until a limiting error is reached. Once F_S and θ are calculated, the remaining forces are also obtained for each slice. Spencer's method is considered very accurate and suitable for almost all kinds of slope geometries and may be the most complete equilibrium procedure. It may also be the easiest method for obtaining the F_s (Duncan and Wright, 2005). Depending on the type of slope analysed, this model is able to establish the failure curve following the typical rotational circle, among other uses (Verruijt, 2010).

The F_S, classically defined as a ratio of stabilizing and destabilizing forces, determines the stability of a slope as follows:

$$F_S = \frac{\sum(Forces\ standing\ against/oppose\ sliding)}{\sum(Forces\ that\ induce\ sliding)} \quad (4)$$

According to limit equilibrium methods, the two equilibrium conditions (forces and moments) must be satisfied. Taking into account these elements, the Fs is then obtained from the following expression (Spencer, 1967):

$$Fs = \frac{1}{\sum W \sin\alpha} \sum[c'b \sec\alpha + \tan\phi' \ (W\cos\alpha - ub\sec\alpha)] \quad (5)$$

Where ϕ′ is the friction angle at the fracture surface, u is the pore pressure at the fracture zone, c′ is the soil cohesion, α is the angle at the base of the slice, W is the external vertical forces and b the width of the slice. According to equations (4) and (5), the slope can be considered unstable if its value of the safety factor 'F_s' is lower than 1, or stable if it is equal o higher than 1. It should be noted that, when applying the factor in the engineering and architecture fields, the limiting value tends to be higher than 1, with common values being 1.2 or even up to 1.5 (Burbano et al., 2009), security coefficients that include The European technical regulations and, specifically, the technical regulations of Spanish application (table 2.1, of the DB-C of the CTE, or Technical Code of the Building) among others. This is just a confidence measure for your calculations. The Fs can also be defined as the ratio between the shear strength (τ), based on the cohesion and the angle of friction values, and the shear stress, based on the cohesion and the internal friction angle required to maintain the equilibrium (τ_{mb}).

As mentioned, the minimum Fs to consider a slope stable is equal to 1. However, several authors (Yong et al., 1977; Van Westen and Terlien, 1996) suggest that the angle of a slope would have to be defined by a value of the Fs superior to the unity to take into account the exogenous factors of the slope. Following Jimenez Salas (1981), a value of $F_S \geq 1.3$ can be considered stable by most standards.

To analyse the slope using the Spencer's method, a set of equations must be solved to satisfy the forces and momentum equilibrium and to obtain the F_S. The values of F_S and θ are the unknowns that must be solved. Some authors suggest that the variation of θ can be arbitrary (Morgenstern y Price, 1965), although the effect of these variations in the final value of F_S is minimal. The variation of the angle depends on the soil's ability to withstand only a small intensity of the shear stress.

Having said that, if we assume that the forces between slices are parallel (in other words, that θ is constant), equations (1) and (2) become the same, resulting in:

$$\sum Q = 0 \tag{6}$$

The assumption that the forces between slices are parallel gives optimal results for the calculation of the critical safety coefficients in equation 5 (Spencer, 1967). To solve these equations, we used the FSOLVE function of the MATLAB software, giving an initial Fs and angle. The FSOLVE function is a tool inside the optimization toolbox from MATLAB that solves systems of nonlinear equations. When using this tool, an initial value must be provided to start the calculation.

When solving the normal and parallel forces at the base of the slice of the five acting forces, we obtain (Q), resulting from the forces between slices:

$$Q = \frac{\frac{c'b}{F}\sec\alpha + \frac{\tan\phi'}{F}(W\cos\alpha - ub\sec\alpha) - W\sin\alpha}{\cos(\alpha-\theta)[1+\frac{\tan\phi'}{F}\tan(\alpha-\theta)]} \tag{7}$$

In this expression, u is the pore pressure (permanent interstitial pressure) at the base of the slice and the weight of the slice is determined by W. If we assume that the soil is uniform and its density (γ) also, the weight of a slice of height h and width b can be written:

$$W = \gamma b h \tag{8}$$

The application of a homogeneous pore pressure distribution (permanent interstitial pressure) has been included in the model (Bishop and Morgenstern, 1960). In this case, the permanent interstitial pressure on the base of the slice was determined by the following expression:

$$u = r_u \gamma h \tag{9}$$

In this expression, u is the pore pressure (permanent interstitial pressure) at the base of the slice, γ is the density of soil, h is the mean height of slice (if the height is not constant) and the weight of it affects the W evaluation.

The pore pressure will be hydrostatic, defined by: $\mathrm{u} = \gamma_{\mathrm{w}}(\mathrm{h} - \mathrm{h_w})$, γ_w is the saturated density of soil, h and h_w is the difference between saturated and dry height. The calculation of the infiltration factor is calculated with the following equation:

$$r_u = \frac{u}{\gamma h} \tag{10}$$

The factor r_u is a coefficient of pore pressure (interstitial pressure coefficient), which determines the rain infiltration factor on the slopes. As it is well known, the water that

infiltrates the soil may produce a modification of the pore pressure, affecting its resistant capacity. This factor may vary from 0 (dry conditions) to 0.5 (saturated conditions). In the article of Spencer (Spencer, 1967), assuming a homogeneous pore-pressure distribution as proposed by Bishop and Morgenstern (1960), the mean pore-pressure on the base of the slice can be written like the equation 7.

This equation is used in our proposed model for calculating the safety factor (substituting the expression of *u* in equation 5).

3. Terrain stability (TS) algorithm and tests

Figure 2 shows the results of applying the Terrain Stability model to an irregular slope, including the initial and final points of the first failure circle (shown in yellow). This circle corresponds with the initial value introduced by the user into the FSOLVE function. The points of the slope are extracted from a DEM model in ArcGIS 10 (Glennon et al., 2008). The slope height is equal to 15 m, and the soil is considered uniform with the following nominal properties: γ= 19500 N/m^3, ϕ = 22º, *c* = 15000 N/m^2, *u* = 0 N/m^2. For the application example of our algorithm in this section, we have used Geotechnical data of a cohesive soil of the Flysch type of Gibraltar, (Vallejo et al., 2002).

The code works as follows: the initial circular failure curve is plotted using the FPLOT tool, as shown in Figure 2 (yellow line). In this example, the center coordinates are equal to xc = 7 m; yc = 14 m and the lower cut with the slope coordinates (P1 point) equal to xt = 0 m, yt = 0 m. The Fs obtained was 1.6, which is, in principle, a stable slope. It must be taken into account that the mass susceptible to sliding must be divided into a sufficient number of slices. This value is entered into our code through the parameter 'N'. In the application example of our algorithm, the sliding mass was divided into N = 500 slices, this value of N is entered into the code by the user, who decides the value of that parameter. The greater the number of slices in which we divide the sliding mass, the calculation will be more accuracy. N = 500 slice, we consider it a balanced value for an optimal calculation, which relates two fundamental parameters (computer calculation capacity / capacity accuracy).

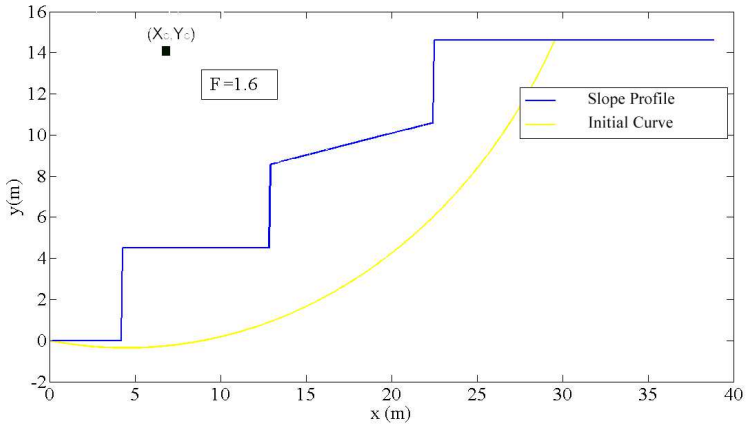

Figure 2. *Idealized cross section of a slope. In this example, the center coordinates are equal to xc = 7 m; yc = 14 m, and the lower cut with the slope coordinates (P1 point) equal to xt = 0 m, and t = 0 m, data that the user introduces.*

The next step is to apply Spencer's method to the different breakage surfaces until the curve with the lowest F_S, is found, and that will be the critical surface susceptible to a circular slip. To determine the minimal Fs using this model, the algorithm calculates the displacement of the lower cutoff point of the critical slip from the slope, as well as the position of the center of rotation of the critical failure curve. In addition, the user must enter a series of possible circular faults. Then, the user introduces the following constraints into the programme: the initial or lower point of the failure curve (P_1) in its intersection point with the slope, which may or may not match the origin of the slope analysed. Another restriction is the centre of the failure circle, (X_c, Y_c), that should initially cut the slope, i.e. the breaking curve must be within the feasible sliding region. With this data, the programme automatically draws a first curve, in this case the yellow line in Figure 3, and calculates the safety coefficient F_s for that initial curve.

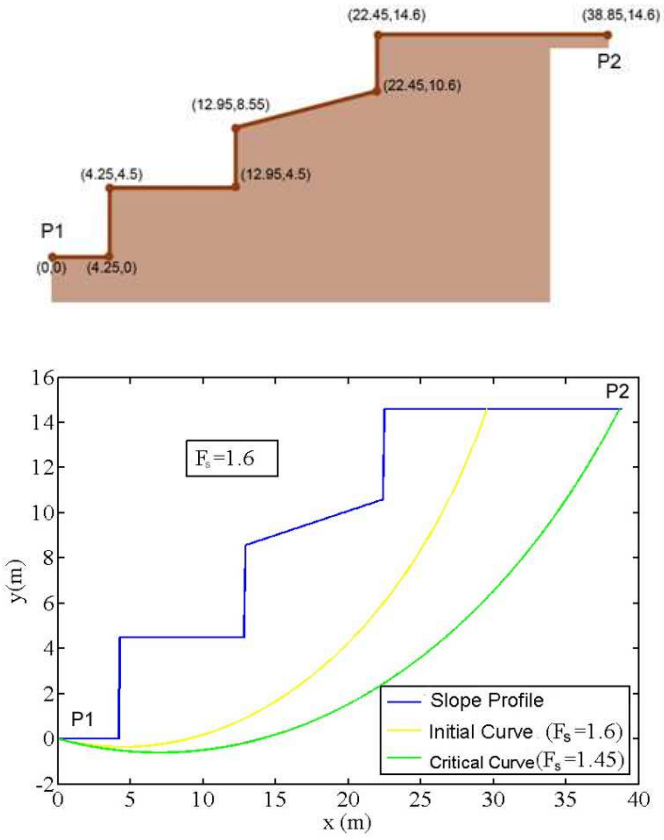

Figure 3. *Results following the application of the software showing the slope profile and surface damage. The F_S and the clearest proof of circular failure are also provided (see the yellow line). P1 coordinates are (0, 0) and P2 (38.85, 14.6) in metres.*

On the basis of this first curve (yellow line in Figure 2), the programme enforces new restrictions:

- The curve passes through the origin of slope P1 = (0, 0).
- The centre of the possible circles of critical breakage is inside the rectangular box defined as: ($x_{box\ min.} < x_c < x_{box\ max.}$; $y_{c\ box\ min.} < y_c < y_{box\ max}$). Note that the coordinates are entered with the 2D expression (X, Y).

Both coordinates of the rotation centre position are free and can change for every circle. From the initial failure curve, characterised by the point x = (x_c, y_c), the MATLAB "fmincon" function is used to obtain a new critical point (x_c*, y_c*) where the Fs from the breakage curve is the minimum provided by fmincon. In this example, starting from the initial curve (yellow curve) with point x = (7, 14), the TS model provides a new point x* = (4.4910, 28.1091, 0) with a new Fs, F_S = 1.45. In this case, the new search has been carried out with the following restrictions in the rectangular box, such as 2 m < x_c < 8 m and 16 m < y_c < 40 m. These restrictions are imposed in order to determine the critical circle. With all these restrictions, and because of the first calculated curve (the yellow curve), the developed model calculates the critical curve among the number of curves selected by the user (500 in this case), as well as the failure circle centre, by applying the fmincon (MATLAB function). This defines the curve with minimum Fs (F_{min}) as the value of F_s (see green curve in Figure 3). When solving this problem, a critical selection is the lower cut-off point of the slope. According to different authors, such as Verruijt (2010) and Castedo et al. (2012), the selected point is the same as the P1 point.

To complete the second phase in the TS model operation, the effect of rain infiltration must be introduced by the coefficient of the pore pressure factor r_u. In this example, the infiltration factor was introduced at the base of each slice to account for the infiltration and pore pressure at the base of the break surface of the slope. If r_u increases, the cohesion of the soil mass of the slope decreases, directly affecting the reduction of the slope's Fs. The result is that a dry slope has a F_S = 1.45, but if including the r_u parameter equal to 0.3, the Fs decreases to a value of F_S = 0.95, that means an Fs below the unity, so an unstable circular failure appears (see Figure 4). Entering the infiltration factor, r_u, in Spencer's method to introduce the infiltration effects in slopes, the geotechnical cutting elements of the analysed soil are reduced, also reducing the values of the F_s, both for the initial yellow curve and the optimum green curve (Figure 3). Note that the initial curve in the run shown in Figure 4 is different from the one in Figure 3, as it depends on the data introduced.

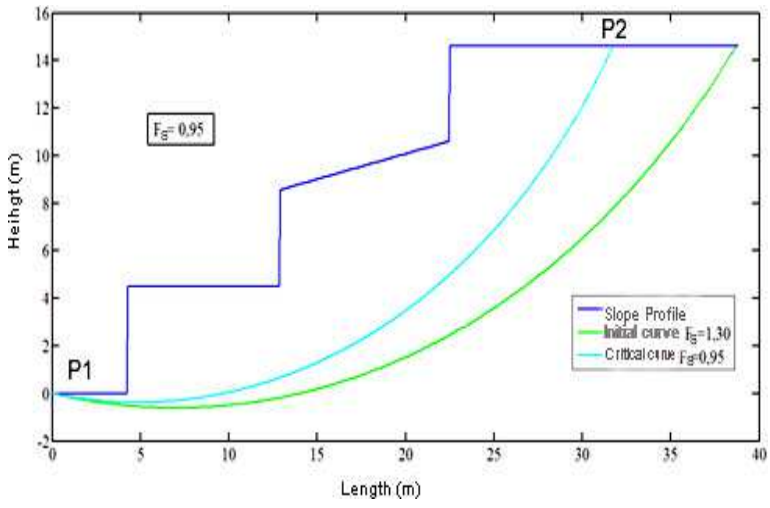

Figure 4. *Outcome of the TS model after the introduction of the infiltration factor, producing an unstable circular failure (Fs = 0.95).*

We can determine that if this infiltration factor value is small enough, taking into account the safety coefficients, the design may still be adequate, but critical information was missing to calculate this parameter.

To clarify the procedure employed in the suggested algorithm, the flowchart (block diagrams) presented in Figure 5 demonstrates the calculation and iteration process as implemented in our software.

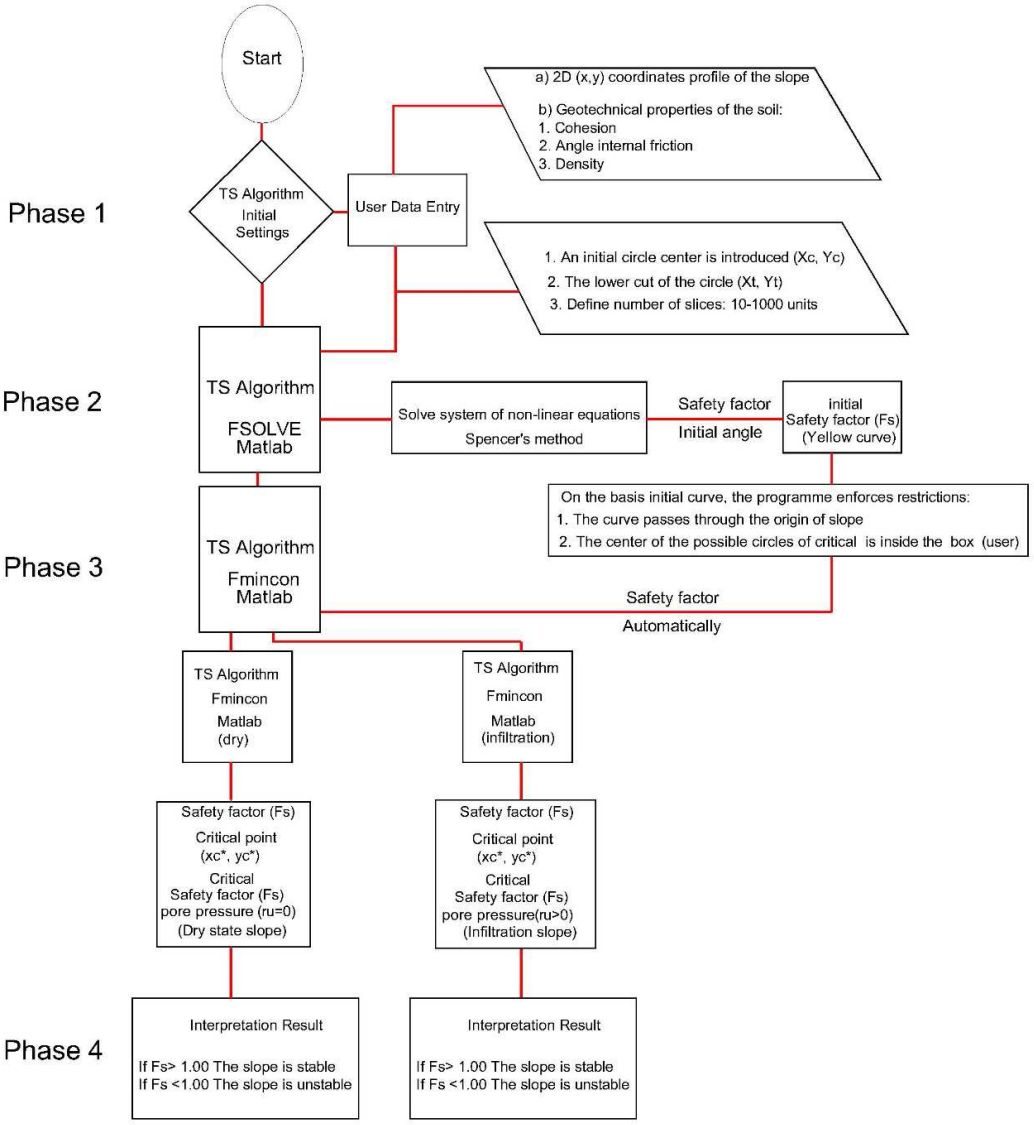

Figure 5. Sequential TS algorithm (block diagrams). Numbers in parentheses refer to numbers in the text.

1. Our algorithm (software) is more versatile compared to the STB 2010, the model developed here can analyze slope from right to left and vice versa, the STB 2010 only allows the analysis from right to left. Other software programmes, like the STB 2010, use a modified version of Bishop's method, a less accurate methodology than Spencer's method. A modified version of Bishop's method solves only the equilibrium in momentum while the Spencer method also considers the equilibrium in forces.

2. Another improvement made by the TS code, in comparison with others, is that the use of the Spencer's method allows us to analyse any type of slope and soil profile. In this procedure, we calculated the worst breaking curve by modifying the calculation points.

3. In the TS model, from the first slip rotational circle obtained in MATLAB, many circles were then calculated using the fmincon function, with some user restrictions. However, other models, like the STB 2010, require the definition of a quadrangular region (to look for the centres of rotational failures) and a point (namely 5, see Figure 9) to define the curve as where the failure must pass. Also, the number of circles that the STB 2010 model can analyse for their minimum value is limited to 100.

4. The TS model can detect relevant earth movements derived from rainfall infiltration, both translational and rotational types (Stead et al., 2006), such as those that usually occur in regions like India, the United States, South America and the United Kingdom, among other places. The programmes that do not contemplate this option will overestimate the Fs, potentially with great errors.

The TS model has an additional advantage: it also offers the opportunity to incorporate, in the same code, the stability analysis and the effect of the infiltration factor in the rainfall regime. This is a step forward from open access programs, such as STB 2010, and also alternative payment software, such as Slide.

4. Example of this application in the municipality of La Viñuela, Málaga, Spain

In 2010, La Viñuela, Málaga, (Spain) experienced torrential rainfall. The main consequence was a devastating landslide with serious personal and material losses, as shown in Figure 6. The coordinates where this event occurred were in degrees (36.88371409801, -4.204982221126).

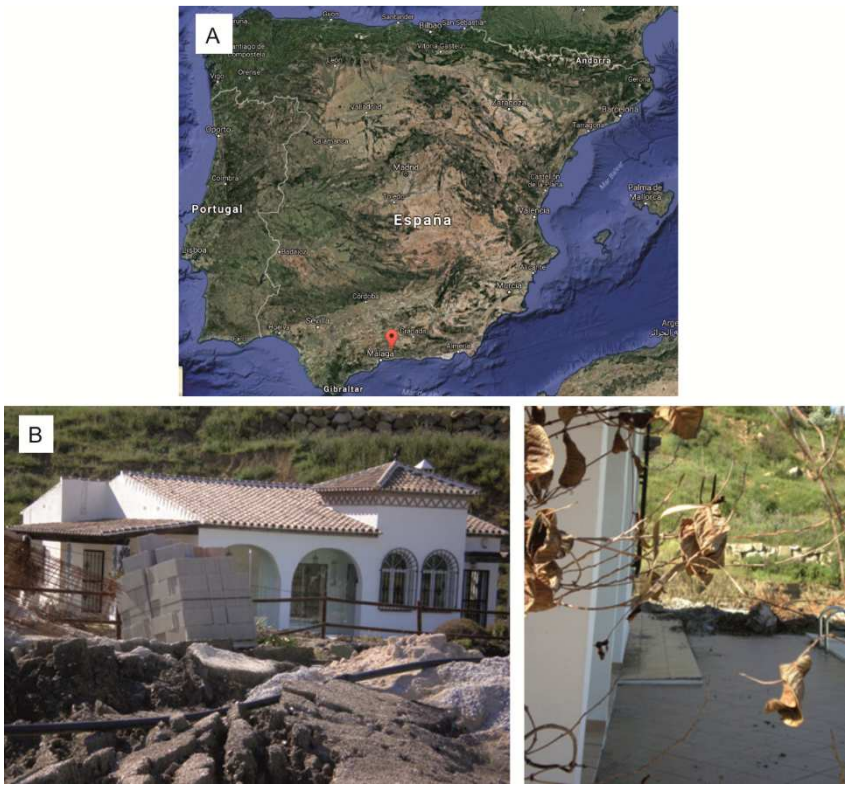

Figure 6. *A) Spanish map with the location of La Viñuela (Google Maps). B) Real images taken by the authors at La Viñuela in 2010.*

4.1 Geological and hydrological environment

The study area is located in the county of La Viñuela, specifically in the Hundidero village, which is located immediately north of the swamp of La Viñuela (El Hundiero) and south of The Baetic System Mountain ranges (South Iberian Peninsula).

According to the Cruden and Varnes' classification (1996), the slide corresponds to a rotational slide-like complex movement because it was generated in two sequences at different speeds. This type of mechanism is characteristic of homogeneous cohesive soils, as was the one analysed here (Cornforth, 2005; Rahardjo et al., 2007; Lu and Godt, 2008).

This event caused serious damage to different buildings. Regarding the damage caused, in the initial stretch of the slope (its head), a house was dragged and destroyed and another was seriously damaged. On the right bank of the mentioned house, another building was affected. In total, this event left a balance of two buildings destroyed and one seriously compromised. Although 15 people lived in these houses, there were no fatalities. About 20 houses were to be constructed at the head of the slope; fortunately, the event happened before this construction. Figure 7 shows an aerial picture from 2006 before the disaster as well as the affected area and landslide in 2010.

Figure 7. *A) An aerial photograph from before the event (2006). B) An aerial photograph taken after the landslide (2010).*

4.2 Event features and geometry

For this example, we used data of IGN, the Spanish National Geographic Institute (http://centrodedescargas.cnig.es/CentroDescargas), and downloaded bit map MTN25, that is a 1:25000 topographic map in ETRS 89 coordinates and UTM projection. The downloaded map is generated in a file by means of a geo-referenced digital rasterization (vector to raster conversion). Specifically, we downloaded page number 1039, which is the one corresponding to the landslide zone of the case study. Figure 8 shows the area of the case study.

From this map we obtained the topographic information to acquire all necessary profiles to study the landslide. Moreover, as our algorithm is a 2D model, with this topographic map we study the critical curve of the slip in the most unfavourable profile of the landslide (Figure 8).

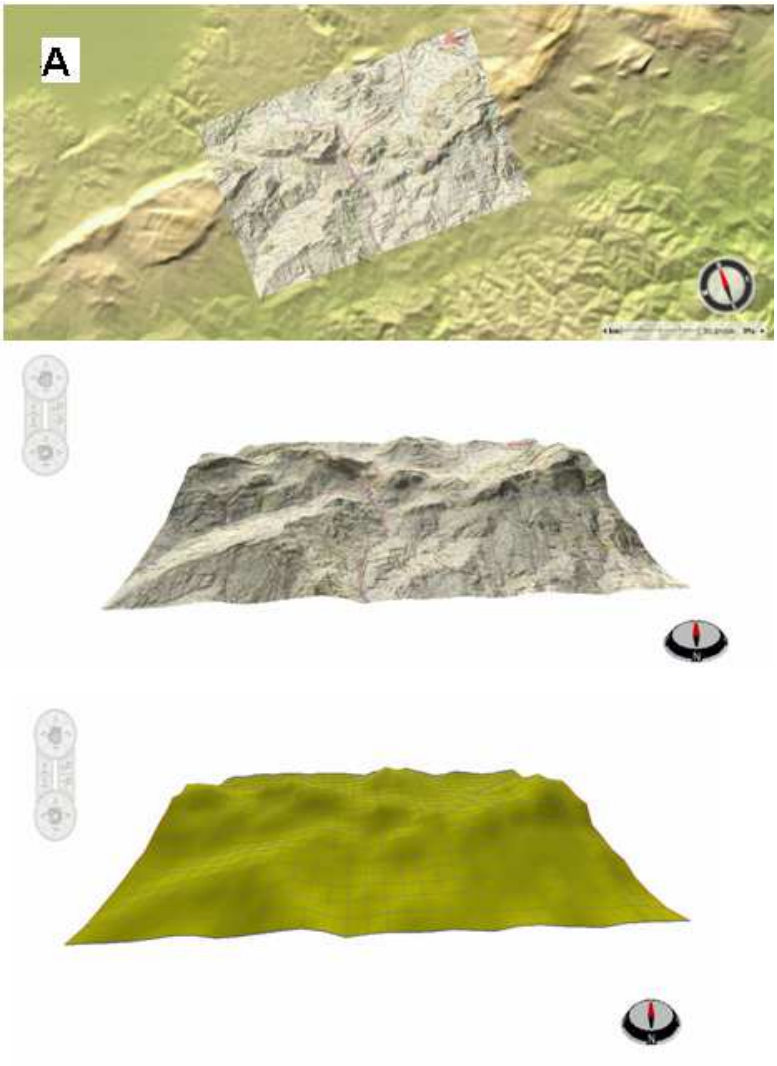

***Figure 8**. A) Topographic map in a GIS map; page number 1039 of the IGN (Spanish National Geographic Institute).*

It is well known that mass movements, such as landslides, are highly complex morphodynamic processes. We selected The Hundidero as our study area because it is prone to landslides. In order to analyse this case study using our model, we first calculated the initial displaced volume of the study area. According to the dimensions of the problem, the initial displaced volume was calculated, equivalent to the volume of half an ellipsoid (Varnes, 1978; Beyer, 1987; Cruden and Varnes, 1996) that is Vol = 1/6 π (width x length x depth). In our particular case, the width was equal to 70 m, the length equal to 235 m and the depth equal to 5 m, making up a total volume of 4.364 m^3 (Figure 9). Taking an average of 33% elongation, as proposed by Nicoletti and Sorriso-Valvo (1991) and Cruden and Varnes (1996), we determined that the total material displaced in this landslide had an approximate volume of 5.804 m^3. In this mass displacement, it is also necessary to consider material added by erosion and dragged from the initial mass displaced. In Figure 7, the straight line indicates the first rotational movement, and the zigzag line shows the planar drag and glide after the first rotational movement. The green region is the total area displaced or affected by mass movement. After the first circular movement, the mass moved rapidly, associated with a continuous rise in incremental pore pressure and the rapid reduction of shear strength, without allowing pressure dissipation.

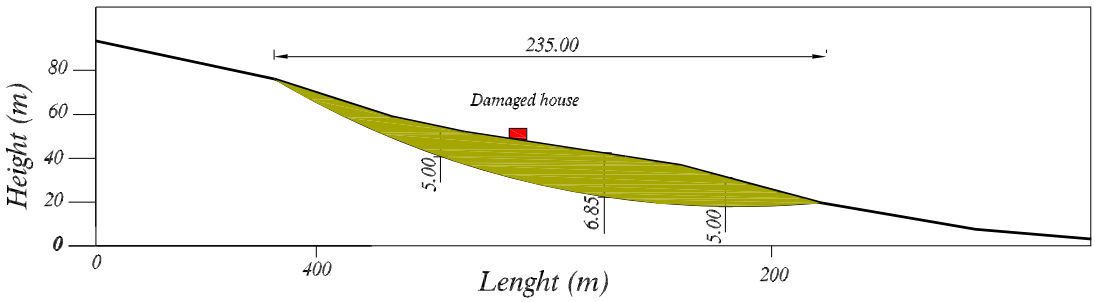

***Figure 9**. Characterisation and longitudinal section of the rotational sliding (Geolen S.A., 2010). The location of the dragged house is noted in red: Analysed by the TS model.*

The initial spit of land had an approximate size of 235 m in length by 70 m in width. Due to this initial displacement, there was a drag and a huge posterior planar displacement of about 550 m length, affecting a zone with several parcels of land and buildings. These sizes were confirmed using aerial photography and field data. The soil is basically composed of clays of variable thicknesses, of fine grain, with fluvial sediments and silty clay. The authors obtained this data by conducting a field survey, as well as through the laboratory tests carried out by the laboratory Geolen S.A. (Geolen, 2010). From a geological and geotechnical point of view, according to a survey of those present as the laboratory extracted the materials, different lithological levels can be distinguished, as shown in Table 1.

***Table 1.** Lithology of the area affected by the failure, according to the laboratory tests of Geolen S.A. No groundwater level was detected.*

Level/layers	Lithology	Depth (m)

LEVEL 1	Silty sand with natural schistose pebbles	0.90
	Silty clay with marl intercalations	4.20
LEVEL 2	Colmenar unit, upper oligocene–lower miocene	
	Sandy clay	9.00
LEVEL 3	Colmenar unit, upper oligocene–lower miocene	(*end of the probe*)

The laboratory tests included a sieve analysis (following UNE 103 101) in three of the samples extracted from the field, at depths of 1.80–2.00 m, of which 70.3% was composed of clay and silt; according to this, the sample is classified as cohesive. The liquid limit and the plastic limit were determined on two of the samples (following UNE 103 103 and UNE 103 104, respectively), yielding liquid limit values of 57.5% and 64.2% and a plasticity index of 37%, respectively. According to the lab results, the material can be classified as high plasticity material with the potential of having a high water content. The landslide analyzed began in February 2010, ending in March of that same year. However, based on the field inspection and the analysis of the rainfall series in the La Viñuela region in 2010 (see Figure 10), it can be inferred that the main causes of the event were:

- The poor geomechanical parameters of the material that formed the affected hillside, and
- The hydrometeorological conditions in the days preceding and days after the event, according to the histogram.

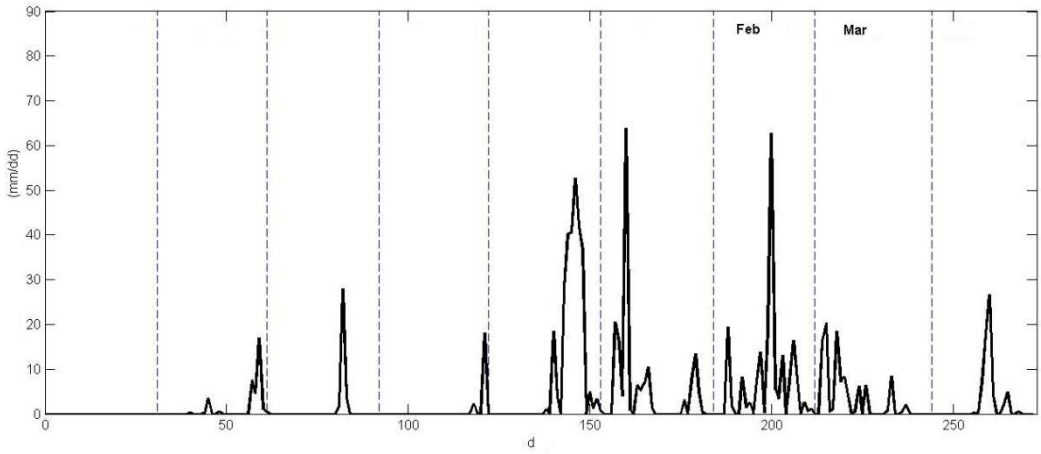

***Figure** 10. Rainfall histogram at La Viñuela from August 2009 to April 2010. Rainfall data has been provided by the Spanish Meteorological Agency (Station of Viñuela).*

Most of the landslides observed during these days occurred as a consequence of exceptionally intense rainfalls. The precipitation data was provided by the meteorological station of La Viñuela (Figure 10). It can be observed that large amounts of precipitation fell during the months of December, January, February and March of 2010, with peaks of most 60 l/m2 in a single day (January and February). In total, 890 l/m2 fell in the 2009-2010 hydro cycle, which ended at the end of April 2010. This is a key point in slope stability to consider when dealing with areas capable of having high infiltration rates.

The rotational slide analysed had occurred between level 2 and level 3, when the water content reached that depth, as confirmed by the infiltration calculations in the terrain (see graphs in Figure 9, reaching depths of up to 5 m). Two direct shear tests (consolidated and drained) were conducted in unaltered samples extracted from the boreholes at 3.00–3.60 m and 4.00–4.60 deep. The cut-off values of the soil are specified in Table 2. Those values were used in the developed software to obtain the safety coefficient and the theoretical failure curve.

Table 2. *Summary chart of the characteristics of the soil analysed at the GEOLEN S.A. laboratory: ϕ the angle of internal friction, c the cohesion, γ_{Sat} the saturated specific gravity and γ_a the apparent specific gravity.*

Soil parameter	Result	Units
ϕ	17	º
C	0.27	N/mm^2
γ_{Sat}	2000	N/mm^3
γ_a	1650	N/mm^3

The dynamic and continuous tests were carried out by the Geolen S.A. laboratory with an automatic penetrometer ROLATEC ML-60 A type. The data obtained was transcribed by the number of strokes to advance the 20 cms tip, which is called the "penetration number" (N_{20}).

This test is included in the ISO 22476-2:2005 standard as a dynamic probing super heavy, and consists of penetrating the ground with a conical tip of standard dimensions. The depth of the failed mass can be estimated, as well as the theoretical failure curve for an increase in the soil consistency (see data in Table 3).

The change in the geomechanical response of the soil takes place at a depth of 4–5 m, according to the results of N_{20} and US (samples without changes) taken along the analysed column. In this case, the sloped ground mass showed a characteristic striking relationship of a displaced terrain (Gonzalez de Vallejo et al., 2002). This differs from the underlying or unmoved terrain, which indicated a more consistent striking relationship that was taken within the area of the landslide behind the house drawn in accordance with the analysis of the hits N_{20} from Table 3.

Table 3. *Summary chart of the soil analysed at the GEOLEN S.A. laboratory. Bold values show, according to the data of the field penetrometers, the depth mobilized by the rotational sliding.*

Depth (m)	Hits N_{20}	Consistency	Admissible stress (N/mm^2)
0.00 – 1.00	**4**	**Soft**	**0.03**
1.00 – 2.00	**3**	**Soft**	**0.02**
2.00 – 3.00	**6**	**Slightly hard**	**0.04**
3.00 – 4.00	**7**	**Slightly hard**	**0.05**
4.00 – 5.00	**10**	**Slightly hard**	**0.07**
5.00 – 6.00	19	Moderately hard	0.12
6.00 – 7.00	52	Hard	0.31
7.00 – 8.00	63	Hard	0.35
8.00 – 8.60	84	Hard	0.44

4.3 Input data

To analyse the topography of the critical section, we obtained the DEM data from ArcGIS 10 software programme (Esri, 2010), with a scale of 1:1000, through Spanish National Geography Institute (IGN) raster maps, with adequate accuracy. These data were interpolated to a 2 m grid using a triangulated network interpolation methodology. Orthophotos proved very useful to locate the landslide with accuracy and to validate the field survey. The model developed here applies to failure in an initiation zone, in addition to predicting landslides, including those induced by the infiltration of critical rains.

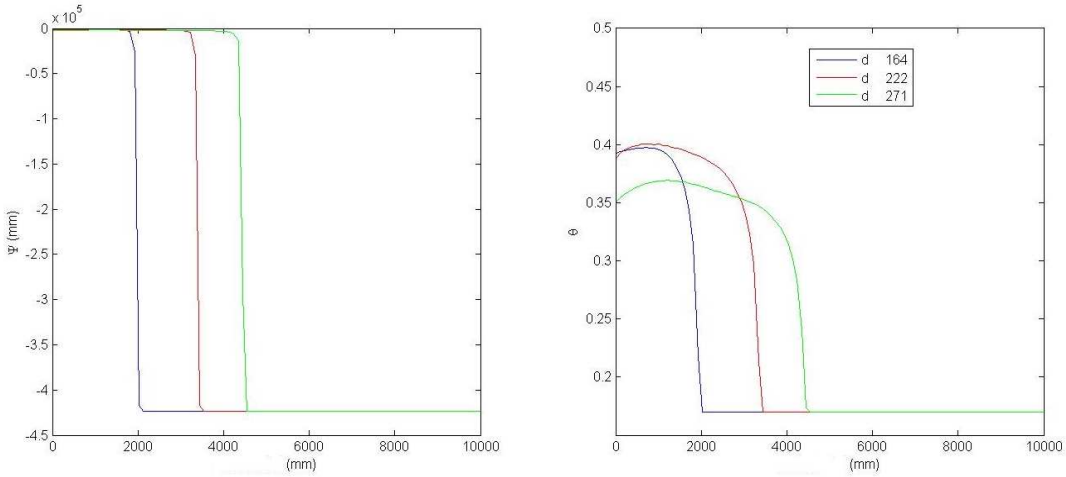

Figure 11. *Left: hydraulic potential. Right: volumetric water content. Both have been plotted as a function of the depth (mm) at different times (d).*

To complete the input data, we plotted the hydraulic potential and the volumetric water content, as a function of depth in the ground for different time steps, using a previously developed infiltration model, as shown in Figure 11 (Herrada et al., 2014). The figure shows the evolution of how the wetting front advances can be observed. These reached almost 5 m deep at the end of April 2010.

4.2 Analytical results

We applied the TS model using topographic data obtained from the ArcGIS 10 software program. We did so to obtain the degree of stability of the sliding land based on the angle of internal friction, the cohesion, the density and the angle of the slope we analyzed. Figure 9 shows the analytical results from the real slope, by studying and analyzing the most unfavorable profile of the landslide studied. In addition we compared the results given by the developed TS model and the results given by STB 2010 model, using free surfaces in both cases. In our model the worst curve (shown in green) was calculated automatically from the initial curve (show in blue), resulting in F_S = 2.300, in the dry state (Figure 12).

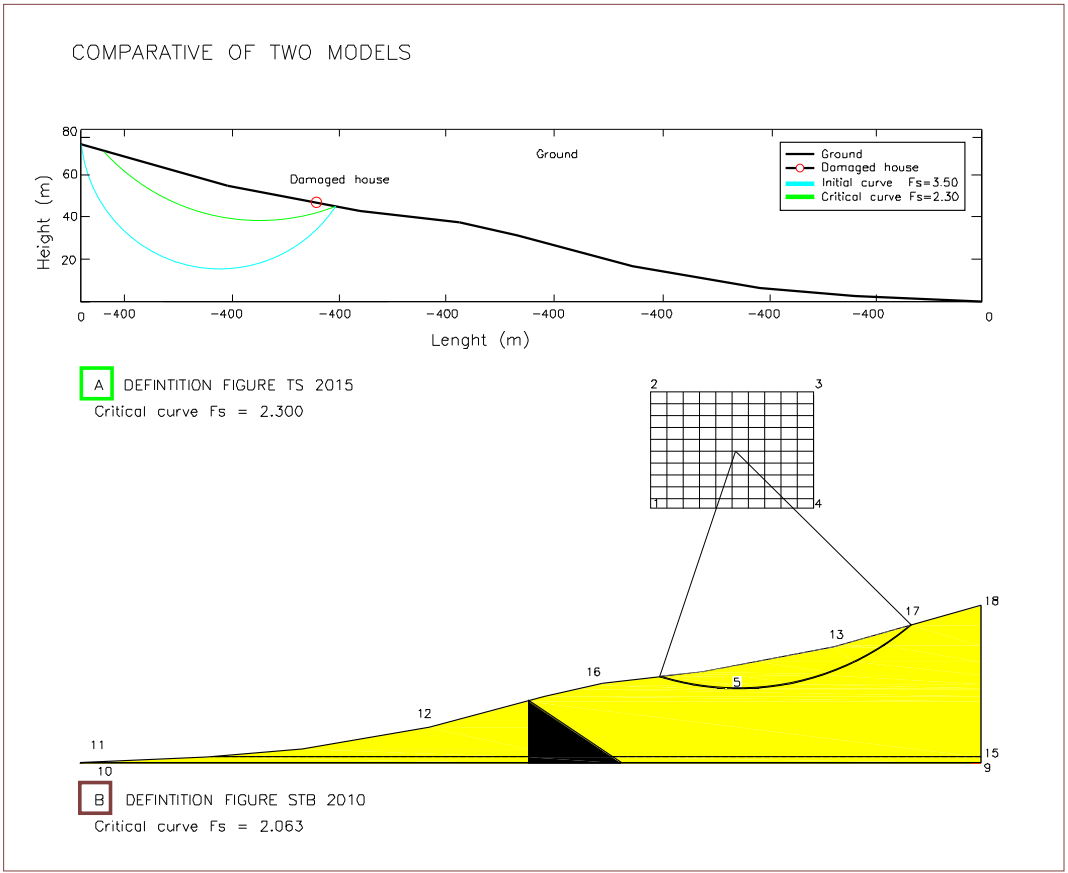

504

505 ***Figure 12.*** *Top: TS model with a critical failure of F_S = 2.300. Bottom: results from the STB 2010 model*
506 *with an Fs of 2.063.*

507 As can be noted, the failure curves are similar, and the safety coefficients F_S only differ by
508 0.237. In both cases, the results indicated are conservative estimates, resulting in a stable
509 slope that was not realistic, as was the case in La Viñuela. In order to get the most
510 unfavourable curve, which would match the analysis of the actual event, the pore coefficient
511 must be introduced. At the first runs of the model, the r_u was equal to zero (dry soil – Figure 9),
512 but if this value is changed to r_u = 0.35, the results are quite different (Figure 13). The resulting
513 failure was near the surface and the top cut with the slope found relatively near the houses.
514 Taking into account the infiltration of rainwater, the slope analysed in the TS model showed a
515 value of F_S = 0.98, in other words, that it was unstable.

516 This calculation and the theoretical failure curve provided by our model was able to reproduce,
517 in a realistic way, the landslide which occurred in La Viñuela. Our model found that the critical
518 surface area that corresponded with the profile of the terrain was 12.927.45 m^2, which closely
519 matches the real situation. In the STB 2010 programme, it was 7.825.35 m^2; therefore, our
520 prediction was more accurate.

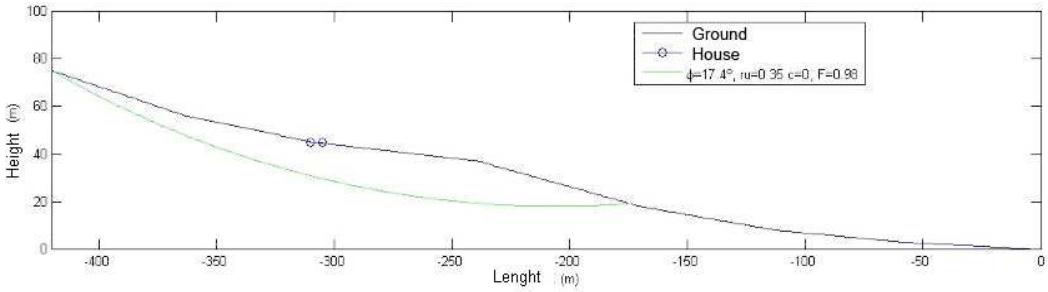

Figure 13. *A new calculation including the pore coefficient r_u showing the worst curve in green. The circles show the houses dragged by the landslide.*

As mentioned, the STB 2010 model does not allow stability calculations to apply to rainfall infiltration on a hillside. Hence, it is not capable of predicting a hillside's instability in a critical rainfall scenario, which was critical in the slope analysed. The STB 2010 model found that the hillside studied had an Fs of F_S = 2.063; that means it was a very stable slope. Consequently, our original algorithm TS model appears to be more efficient and accurate.

If we compare the results of the penetrometric tests (Table 3) and the laboratory tests (Geolen 2010) summarized in the actual critical surface in the most unfavourable profile of landslide (Figure 9), with those offered by our algorithm TS (Figure 13) to which we apply the infiltration factor r_u=0.35, (high interstitial pressure) we can check the similarity between the two critical surface of the landslide.

A value of r_u = 0.35 has been introduced in the calculation and the code gave us a value of the slope safety factor of Fs = 0 .95 (unstable), when in the dry state the code calculated a safety factor of Fs = 2.300 (stable). The calculation of the safety factor in the STB 2010 program; that lacks the analysis of infiltration in the calculation, offered a result of Fs = 2.063 (stable).

Using the STB 2010 program, we would not have been able to previously detect the landslide of the case study of the paper, calculation that is not normally done in the stability calculations; with the calculation with our code we could have avoided the collapse of the building.

With these results, The Terrain Stability analysis performed using the developed model defines fairly well the slip-breaking curve that intuitively appears to be susceptible to failure, especially when heavy rains occur. As an example, the landslides which occurred in the La Viñuela area could only have been predicted if the infiltration had been taken into account. Even then, it could not have been done with other available software programmes, which were not able to consider it.

5. Conclusion

The terrain stability (TS) analysis defines fairly well the critical surface to landslide in 2D of each profile of the analyzed slope and the safety slip factor (Fs). We developed this model due to the need for a useful tool to predict landslides, especially when heavy rains occur.

The TS model we developed uses the Spencer's method, which is more precise than the modified Bishop method, model used by other software such as the case of the STB 2010, so it

554 differs in the results it provides for the F_S. It also takes into account the factor of water
555 infiltration due to critical rains, which other software programmes do not consider. A failure
556 surface can be determined by constraints using the MATLAB function fmincon. The data
557 needed to run the model include soil and climate properties that may vary in space and time.
558 The exit indices of the analysis (F_S) should be interpreted in terms of relative risk. The methods
559 implemented in the TS model are based on data structures, which are based on the data entry
560 of the elevation model (DEM), so we obtain a topographic map, a key element to obtain the
561 topographic profile to be studied with our algorithm.

562 In the case study analysed, the slope was initially stable and was so determined by the analysis
563 performed with the STB 2010 model. However, the slope became unstable due to the heavy
564 rains of that hydrological period, which called for the application of the pore pressure
565 coefficient r_u. For analysing cases of heavy rain, this model is a powerful tool for determining
566 slope stability. In addition, thanks to the great versatility of this model, it is applicable to any
567 analysis in other parts of the world, based on the methods of limit equilibrium (Spencer, 1967).
568 The TS model can also be used in combination with GIS software, SINMAP, TRIGRS model and
569 aerial photographic analysis, as well as mapping techniques or even as part of other models
570 like the coastal recession models (Castedo et al., 2012).

571 ## 6. References

572 Aenor Institut: Geotechnical investigation and testing - Field testing - Part 2: Dynamic
573 probing (ISO 22476-2:2005), Madrid, Spain, 2008.

574 Aleotti, P.: A warning system for rainfall-induced shallow failures, Eng. Geol. 73:247–
575 265, 2004.

576 Alvioli, M., Baum, R. L.: Parallelization of the TRIGRS model for rainfall-induced
577 landslides using the message passing interface, Environmental Modelling & Software 81, 122-
578 135, http://dx.doi.org/10.1016/j.envsoft.2016.04.002, 2016.
579
580 Anbalagan, R.: Landslide hazard evaluation and zonation mapping in mountainous
581 terrain, Eng. Geol. 32, 269–277, 1992.
582
583 Anderson, M. G., Howes, S.: Development and application of a combined soil water-
584 slope stability model. Q. J. Eng. Geol. London, 18: 225-236, 1985.
585
586 Ayalew, L., Yamagishi, H., Ugawa, N.: Landslide susceptibility mapping using GIS-based
587 weighted linear combination, the case in Tsugawa area of Agano River, Niigata Prefecture,
588 Japan, Landslides 1, 73–81, 2004.
589
590 Acharya, K. P., Bhandary, N. P., Dahal, R. K., Yatabe, R.: Seepage and slope stability
591 modelling of rainfall-induced slope failures in topographic hollows, Geomatics, Natural Hazards
592 and Risk, 7:2, 721-746, DOI:10.1080/19475705.2014.954150, 2016a.
593
594 Acharya, K. P., Yatabe, R., Bhandary, N. P., Dahal, R. K.: Deterministic slope failure
595 hazard assessment in a model catchment and its replication in neighbourhood terrain,
596 Geomatics, Natural Hazards and Risk, 7:1, 156-185, DOI:10.1080/19475705.2014.880856,
597 2016b.

598

Ayenew, T., Barbieri, G.: Inventory of landslides and susceptibility mapping in the Dessie area, Northern Ethiopia, Eng. Geol. 77, 1–15, 2004.

Baum, R. L., Savage, W. Z., Godt, J. W.: TRIGRS-A Fortran program for transient rainfall infiltration and grid-based regional slope-stability analysis, Version 2.0. US geological survey open-file report 424, 38 https://pubs.usgs.gov/of/2008/1159/, 2008.

Bishop, A. W., Morgenstern, N. R.: Stability coefficients for earth slope, Geotechnique 10, 129-150, 1960.

Bishop, A. W.: The Use of the slip circle in the Stability Analysis of Slope, Geotechnique 5: 1:7-16, 1955.

Beyer, W. H.: Handbook of Mathematical Sciences. 6th ed., Boca Raton/Florida, 1987.

Bisson, M., Spinetti, C., Sulpizio, R.: Volcaniclastic flow hazard zonation in the sub-apennine vesuvian area using GIS and remote sensing, Geosphere 10, http://dx.doi.org/10.1130/GES01041.1, 2014.

Borselli, L.: SAPP 4.2.0.: Advanced 2D Slope stability Analysis by LEM by SSAP software, SSAP code Manual, version 4.2.0, available at: http://www.Ssap.Eu/Manualessap2010.Pdf., 2012.

Burbano, G., del Cañizo, L., Gutiérrez, J. M., Fort, L., Llorens, M., Martínez, M., Paramio, J. R., Simic, D.: Guía de cimentaciones en obras de carretera, Ministerio Fomento, Madrid, 2009.

Canili, E., Mergili, M., Thiebes, B., Glade, T.: Probabilistic landslide ensemble prediction systems: lessons to be learned from hydrology, Nat. Hazards Earth Syst. Sci., 18, 2183–2202. https://doi.org/10.5194/nhess-18-2183-2018, 2018.

Carrara, A., Cardinali, M., Guzzetti, F., Reichenbach, P.: GIS technology in mapping landslide hazard. In: Carrara, A., Guzzetti, F. (Eds.), Geographical Information System in Assessing Natural Hazard, Kluwer Academic Publisher, Netherlands, 135–175, 1995.

Casagli, N., Catani, F., Puglisi, C., Delmonaco, G., Ermini, L., Margottini, C.: An inventory-based approach to landslide susceptibility assessment and its application to the Virginio River Basin, Italy, Environ. Eng. Geosci. 3, 203–216, 2004.

Castedo, R., Murphy, W., Lawrence, J., Paredes, C.: A new process–response coastal recession model of soft rock cliffs, Geomorphology, 177, 128-143, 2012.

Cheng, Y. M., Lansivaara, T., Wei, W. B.: Two-dimensional slope stability analysis by limit equilibrium and strength reduction methods, Computers and Geotechnics 34, 3, 137-150, 2007.

Chugh, A. K., Smart, J. D.: Suggestions for slope stability calculations. Computers & Structures 14, 1–2, 43-50, 1981.

Collison, A., Wade, S., Griffiths, J., Dehn, M.: Modelling the impact of predicted climate change on landslide frequency and magnitude in SE England. Eng. Geol. 55, 205–218, 2000.

644 Crosta, G. B., Frattini, P.: Distributed modelling of shallow landslides triggered by
645 intense rainfall, Natural Hazards and Earth System Sciences (2003) 3: 81–93, 2003.
646
647 Crozier, M. J., Glade, T.: Landslide hazard and risk: issues, concepts, and approach. In:
648 Glade, T., Anderson, M., Crozier, M. (Eds.), Landslide Hazard and Risk. Wiley, Chichester, 1–
649 40, 2005.
650
651 Cruden, D. M. and Varnes, D. J.: Landslides types and processes. In: Landslides
652 investigation and mitigations, Transportation Research Board Special report 24, Turner y
653 Shuster eds., 36-75, 1996.

654 CTE: Technical building Code, Basic Document Structural Safety DB-SE. Ministry of
655 Development, Spain, available at: https://www.codigotecnico.org/, 2007.

656 Dai, F. C., Lee, C. F.: Terrain-based mapping of landslide susceptibility using a
657 geographical information system: a case study, Can. Geotech. J. 38, 911–923, 2001.

658
659 Dai, F. C., Lee, C. F., Ngai, Y. Y.: Landslide risk assessment and management: an
660 overview. Eng. Geol. 64, 65–87, 2002.
661
662 Duncan, J. M., Wright, S. G.: Soil Strength and Slope Stability, John Wiley, Hoboken,
663 N. J., 2005.

664 Duncan, J. M.: Landslide Types and Processes. Landslides investigations and mitigation.
665 Ed. Turner A. Special Report, TRB., 1996.

666 Environmental Systems Research: Institute Geographic information system (platform
667 and resources ArcGIS), California, EEUU, available at: http://www.esri.es/arcgis/productos/,
668 2017.

669 Fall, M., Azzam, R., Noubactep, C.: A multi-method approach to study the stability of
670 natural slopes and landslide susceptibility mapping, Eng. Geol. 82, 241–263, 2006.
671
672
673 Fellenius W.: Calculation of the stability o Heat dams. Washington, D.C.: In Proceeding
674 of the 2nd Internacional Congress on Large Dams, - Vols. 4, 445. -4:445, 1936.

675 Geolen Engineering: Geotechnical study in the Viñuela. Sevilla, Spain, availble at:
676 http://www.geolen.es, 2010.

677 Girma, F., Raghuvanshi, T. K., Ayenew, T., Hailemariam, T.: Landslide hazard zonation in
678 Ada Berga District, Central Ethiopia – a GIS based statistical approach, J. Geomatics 90, 25–38,
679 2015.

680 Glennon, R., Harlow, M., Minami, M., Booth, B: ArcGis 9. ArcMap Tutorial. Esri North
681 Carolina. U.S.A., 2008.

682 González de Vallejo, L., Ferrer, M., Ortuno, L., Oteo, C.: Ingeniería Geológica. Madrid:
683 Prentice Hall, 2002.

Griffiths, D. V., Marquez, R. M.: Three-dimensional slope stability analysis by elasto-plastic finite elements. Géotechnique 57, Nº. 6, 537–546, 2007.

Griffiths, D. V.: Slope stability analysis by finite elements. A guide to the use of Program slope 64, Geomechanics Research Center Colorado School of Mines, available at: http://inside.mines.edu/~vgriffit/slope64/slope64_user_manual.pdf, 2015.

Guha-Sapir, D., Hargitt, D., and Hoyois, G.: Thirty years of natural Disasters 1974 – 2003: The Numbers, Centre for Research on the Epidemiology of Disasters, available at: http://www.unisdr.org/eng/library/Literature/8761.pdf, 2004.

Gutiérrez-Martín, A.: El agua de infiltración de lluvia, agente desestabilizador de taludes en la provincia de Málaga. Modelos constitutivos, Doctoral Thesis, University of Granada, 2015.

Guzzetti, F., Carrara, A., Cardinali, M., Reichenbach, P.: Landslide hazard evaluation: a review of current techniques and their application in a multi-scale study, central Italy. Geomorphology 31 (1–4), 181–216, 1999.

Herrada, M. A., Gutiérrez-Martin, A., Montanero, J. M.: Modeling infiltration rates in a saturated/unsaturated soil under the free draining condition. Journal of Hydrology, 515, 10–15, 2014.

Hoek, E., Bray, J.W.: Rock Slope Engineering (revised thirded.), Inst. of Mining and Metallurgy, London, 1981.

Iverson, R. M.: Landslide triggering by rain infiltration. Water Resources Research 36(7): 1897-1910, 2000.

Janbu, N.: Stability analysis of slopes with dimensionless parameters. In: Harvard University soil mechanics series, vol 46, 1954.

Jiménez Salas, J. A., Justo Alpañes, J.L.: Geotecnia y Cimientos II, Ed. Rueda, Madrid, 1981.

Jia, G. J., Tian, Y., Liu, Y., Zhang, Y.: A static and dynamic factors-coupled forecasting model of regional rainfall-induced landslides: A case study of Shenzhen, Science China: Technological Sciences 51. Suppl. 2, 164-175, 2008.

Johari, A., Mousavi, S.: An analytical probabilistic analysis of slopes based on limit equilibrium methods, Bulletin of Engineering Geology and the Environment, 1-15, 2018.

Khan, M. E.: The Death Toll from Natural Disasters: The Role of Income, Geography, and Institutions, Review of Economics and Statistics 87, 2, 271-284, 2005.

Leroi, E.: Landslide risk mapping: problems, limitation and developments. In: Cruden, Fell (Ed.), Landslide Risk Assessment. Balkema, Rotterdam, 239–250, 1997.

Liu, S. Y., Shao, L. T., Li, H. J.: Slope stability analysis using the limit equilibrium method and two finite element methods. Computers and Geotechnics 63, 291-298, 2015.

722 Lu, N., Godt, J.:Infinite slope stability under steady unsaturated seepage conditions.
723 Water Resources Research, Vol. 44, W11404, doi:10.1029/2008WR006976, 2008.
724
725 Martelloni, G, Segoni, S, Fanti, R., Catani, F.: Rainfall thresholds for the forecasting of
726 landslide occurrence at regional scale. Landslides DOI: 10.1007/s10346-011-0308-2, 2011.
727
728 Martelloni, G., Bagnoli, F.: Infiltration effects on a two-dimensional molecular
729 dynamics model of landslides, Nat. Hazards, 73(1):37–62, 2014.
730
731 Martelloni, G., Bagnoli, F., Guarino, A.: A 3D model for rain-induced landslides based
732 on molecular dynamics with fractal and fractional water diffusion, Commun Nonlinear Sci
733 Numer Simulat, 50:311–329, 2017.
734
735 Mergili, M., Marchesini, I., Rossi, M., Guzzetti, F., Fellin, W.: Spatially distributed three
736 dimensional slope stability modelling in a raster GIS, Geomorphology 206: 178-195.
737 http://doi.org/10.1016/j.geomorph.2013.10.008, 2014a.
738
739 Mergili, M., Marchesini, I., Alvioli, M., Metz, M., Schneider-Muntau, B., Rossi, M.,
740 Guzzetti, F.: A strategy for GIS-based 3-D slope stability modelling over large areas,
741 Geoscientific Model Development 7 (6), 2969-2982 http://doi.org/10.5194/gmd-7-2969-2014,
742 2014b.
743
744 Michel, G. P., Kobiyama, M., Fabris, R.: Comparative analysis of SHALSTAB and SINMAP
745 for landslide susceptibility mapping in the Cunha River basin, southern Brazil, Journal of Soils
746 and Sediments 7. 1266–1277, 2014.

747 Michel, G. P., Kobiyama, M., Fabris, R.: Critical rainfall to trigger landslides in Cunha
748 River basin, southern Brazil, Natural Hazards 75, 2369-2384, 2015.

749 Montgomery, D., Dietrich, W.: R-SHALSTAB: A digital terrain model for mapping
750 shallow landslide potential, to be published as a technical report by NCASI, available at:
751 http://calm.geo.berkeley.edu/geomorph/shalstab/index.htm,https://grass.osgeo.org/grass74/
752 manuals/addons/r.shalstab.html., 1998.
753
754 Morgenstern, N. R., Price, V. E.: The analysis of the stability of general slip surfaces,
755 Geotechnique 15, 79-93, 1965.

756 National Geographic Institute: Geological and raster maps. Madrid, Spain, available
757 at: http://www.ign.es/web/ign/, 2017.

758 Nicoletti, P. G., Sorriso-Valvo, M.: Geomorphic controls of the shape and mobility of
759 rock avalanches, GSA Bulletin 103 (10): 1365-1373, 1991.

760 Pack, R. T., Tarboton, D. G., Goodwin, C. N.: Assessing Terrain Stability in a GIS using
761 SINMAP. In: 15th annual GIS conference, GIS 2001, Vancouver, British Columbia, February 19-
762 22, 2001.
763
764 Parise, M., Jibson, R.W.: A seismic landslide susceptibility rating of geologic units
765 based on analysis of characteristics of landslides triggered by the 17 January, 1994 Northridge,
766 California earthquake, Eng. Geol. 58, 251–270, 2000.
767

768 Raghuvanshi, T. K., Negassa, L., Kala, P. M.: GIS based grid overlay method versus
769 modeling approach – a comparative study for Landslide Hazard Zonation (LHZ) in Meta Robi
770 District of West Showa Zone in Ethiopia, Egypt. J. Remote Sens. Space Sci. 18, 235–250, 2015.

771 Raia, S., Alvioli, M., Rossi, M., Baum, R. L., Godt, J. W., F Guzzetti, F.: Improving
772 predictive power of physically based rainfall-induced shallow landslide models: a probabilistic
773 approach, Geosci. Model Dev. 7 (2), 495-514, https://doi.org/10.5194/gmd-7-495-2014, 2014.
774
775 Ramos Vásquez, A. A.: Análisis de estabilidad de taludes en rocas, Simulación con LS-
776 DYNA y comparación con Slide, Trabajo Fin de Máster, Máster Universitario en Ingeniería
777 Geológica, ETSI Minas y Energía, Universidad Politécnica de Madrid, 2017.

778 Reid, M. E., Christian, S. B., Brien, D. L., Henderson, S. T.: Scoops-3D - Software to
779 analyze Three-Dimensional Slope Stability Throughout a Digital Landscape, Version 1.0,
780 Virginia: U.S. Geological Survey, 2015.
781
782 Rigon, R., Bertoldi, G., Over, T. M.: 2GEOtop: A distributed hydrological model with
783 coupled water and energy budgets, Journal of Hydrometeorology 7 (3), 371-388
784 https://doi.org/10.1175/JHM497.1, 2006.
785
786 Rossi, G., Catani, F., Leoni, L., Segoni, S., Tofani, V.: HIRESSS: A physically based slope
787 stability simulator for HPC applications, Nat. Hazards Earth Syst Sci 13(1):151–66, 2013.
788
789 Simoni, S., Zanotti, F., Bertoldi, G., Rigon, R.: Modelling the probability of occurrence of
790 shallow landslides and channelized debris flows using GEOtop-FS. Hydrol Processes;22(4):532-
791 545. https://doi.org/10.1016/j.proeps.2014.06.006, 2008.
792
793 Spencer, E.: A method of analysis of analysis of the stability of embankments assuming
794 parallel interslice forces, Géotechnique 17, 11-26, 1967.

795 Toya, H., Skidmore, M.: Economic development and the impacts of natural disasters,
796 Economics Letters, 94(1), 20-25. DOI: 10.1016/j.econlet.2006.06, 2007.

797 Tran, T. V., Alvioli, M., Lee, G., An, H. U.: Three-dimensional, time-dependent modelling
798 of rainfall-induced landslides over a digital landscape: a case study. Landslides, 1-14
799 http://doi.org/10.1007/s10346-017-0931-7, 2018.
800
801 SLIDE V5: 2D limit equilibrium slope stability for soil and rock slopes, user's guide,
802 available at: https://www.rocscience.com/, 2018.
803
804 Stead, D., Eberhardt, E., Coggan, J. S.: Developments in the characterization of complex
805 rock slope deformation and failure using numerical modelling techniques, Eng. Geology 83, 1-
806 3:217-235, 2006.

807 Tschuchnigg, F., Schweiger, H. F., Sloan, S. W.: Slope stability analysis by means of
808 finite element limit analysis and finite element strength reduction techniques. Part II: Back
809 analyses of a case history, Computers and Geotechnics 70, 178-189, 2015.

810 Van Westen, C. J., Terlien, M. J. T.: An approach towards deterministic landslide
811 hazard analysis in gis. A case study from Manizales (Colombia), Earth Surface Processes and
812 Landforms 21. 9:853-868, 1996.

Varnes, D. J.: Slope movement types and processes, In R.L. Schuster and R. J. Krizek (Eds.) Landslides: analysis and control. Transportation Research Board. Special report 176: 11-33, 1978.

Varnes, D. J.: Landslide Types and Processes. In: Turner, A.K., Schuster, R.L. (Eds.), Landslides: Investigation and Mitigation, Transportation Research Board Special Report 247, National Academy Press, National Research Council, Washington, D.C., 1996.

Verruijt, A.: STB—SLOPE: Stability Analysis Program. Delft University. Available at: http://geo.verruijt.net, 2010.

Wang, X., Niu, R.: Spatial forecast of landslides in three gorges based on spatial data mining. Sensors 9, 2035–2061, 2009.

Wilkinson, P. L., Anderson, M. G., Lloyd, D. M., Renaud, P. N.: Landslide hazard and bioengineering: towards providing improved decision support through integrated numerical model development, Environment Modelling and software 17:4, 333-344, 2002.

Wilson, R. C., Jayko, A. S.:Preliminary maps showing rainfall thresholds for debris-flow activity, San Francisco Bay Region, California. US Geological Survey Open-File Report 97-745 F, 1997.

Wu, W., Sidle, R. C.:A Distributed Slope Stability Model for Steep Forested Basins. Water Resour. Res., 31(8), 2097–2110, doi:10.1029/95WR01136, 1995.

Yong, R. N., Alonso, E., Tabba, M. M., Fransham, P. B.: Application of Risk Analysis to the Prediction of Slope Stability. Canadian Geotechnical Journal 14, 540-553, 1977.

Zhang, S., Zhao, L., Delgado-Tellez, R., Bao, H.: A physics-based probabilistic forecasting model for rainfall-induced shallow landslides at regional scale, Nat. Hazards Earth Syst. Sci., 18, 969–982. https://doi.org/10.5194/nhess-18-969-2018, 2018.

Zhou, X. P., Cheng, H.: Analysis of stability of three-dimensional slopes using the rigorous limit equilibrium method. Eng Geol 160:21–33, 2013.

Zhu, D. Y., Lee, C. F., Qian, Q. H., Chen, G. R.: A concise algorithm for computing the factor of safety using the Morgenstern–Price method, Canadian Geotechnical Journal, Vol. 42-1, 272-278, https://doi.org/10.1139/t04-072, 2005.